ChemComm

ROYAL SOCIETY OF CHEMISTRY

COMMUNICATION

View Article Online
View Journal | View Issue

Cite this: *Chem. Commun.*, 2023, 59, 1677

Received 6th December 2022,
Accepted 17th January 2023

DOI: 10.1039/d2cc06655f

rsc.li/chemcomm

Determining the oxidation states of dissolved transition metals in battery electrolytes from solution NMR spectra†

Jennifer P. Allen [ab] and Clare P. Grey *[ab]

Dissolved transition metal ions can induce peak shifts in the NMR spectra of degraded battery electrolytes. Here, we exploit this staightforward, accessible method to calculate magnetic moments for dissolved Ni^{2+}, Mn^{2+}, Co^{2+}, and Cu^{2+}; subsequent analysis of dissolution from $LiMn_2O_4$, $LiNiO_2$, and $LiNi_{0.5}Mn_{1.5}O_4$ shows that the dissolved metals are exclusively divalent.

Transition metal dissolution and deposition is a significant contributor to capacity fade in lithium-ion cells.[1–4] There are limited direct measurements of the oxidation states of dissolved transition metals, but such measurements are typically performed *via* XANES of the electrolyte solution and/or separator.[5–10] This yields only an average oxidation state,[7,8] and XANES measurements often require synchrotron access. EPR spectroscopy has been used to distinguish Mn^{2+} from Mn^{3+},[7,11,12] although this assumes all Mn^{2+} is EPR-observable and all inconsistency between EPR and ICP-OES results is due to the presence of EPR-silent Mn^{3+}—an approach which has been questioned due to the potential EPR silence of some Mn^{2+} complexes.[13] More generally, EPR of metals with either rapid electronic relaxation or with integer spins, S, including Co^{2+} (S = 3/2) and Ni^{2+} complexes (S = 1),[14] can be challenging.[15] Capillary electrophoresis is a promising method that has been used to determine oxidation states of dissolved Mn,[16] Fe,[17] and Cu.[18] Electrochemical methods may also be used to infer metal oxidation states.[19–21]

It is thought that most 3d metals dissolve from cathodes as M^{2+};[10,22–25] however, this is of increasing debate. While EPR, XANES, and electrochemical studies[7,8,11,12,21] of $LiMn_2O_4$ and/or $LiNi_{0.5}Mn_{1.5}O_4$ have observed some fraction of dissolved Mn^{3+}, other XANES, XPS, and capillary electrophoresis/UV-visible studies have shown only Mn^{2+}.[5,9,16] XANES of $LiNi_{0.5}Mn_{0.3}Co_{0.2}O_2$ found dissolved Ni^{2+} and Mn^{2+} but Co^{3+};[6] XANES of $LiNi_{0.33}Mn_{0.33}Co_{0.33}O_2$ found dissolved Mn^{2+} (and deposited Mn^{2+}, Ni^{2+}, and Co^{2+}).[10] Dissolved Cu^{+} and Cu^{2+} (from current collectors) and Fe^{2+} and Fe^{3+} (from $LiFePO_4$) have all been observed.[17,18]

Most of the dissolved metal ions are paramagnetic and in the NMR spectra of electrolytes containing these metals, the paramagnetic species cause bulk magnetic fields and changes in all NMR chemical shifts away from their positions in diamagnetic solutions, known as bulk magnetic susceptibility (BMS) shifts. These BMS shifts are not observed with an internal reference, as the reference is also affected, but it may be observed if the reference is not in contact with the paramagnetic solution, *e.g.*, by using a sufficiently thick-walled solvent capillary.[14,26,27] For a cylindrical sample in a superconducting magnet, neglecting the diamagnetic contribution, the molar magnetic susceptibility of a paramagnetic solute (χ_M, mL·mol^{-1}) depends on the BMS shift it induces ($\Delta\nu$, Hz), the spectrometer frequency (ν_0, Hz), and the metal concentration (c, mol·mL^{-1}) *via* eqn (1).

$$\chi_M = \frac{3\Delta\nu}{4\pi\nu_0 c} \quad (1)$$

If the temperature T is known, then the effective magnetic moment μ_{eff} can be calculated (eqn (2)) and compared to the theoretical spin-only magnetic moment μ_s, which is dependent on the number of unpaired electrons n (eqn (3)).[14,28] Hence, μ_{eff} may permit identification of the oxidation state and spin state of paramagnetic compounds.

$$\mu_{eff} = \sqrt{\frac{3k_B}{N_A{\mu_B}^2}\chi_M T} = 2.83\sqrt{\chi_M T} \quad (2)$$

$$\mu_s = \sqrt{n(n+2)} \quad (3)$$

Notably, μ_s does not account for spin–orbit coupling or orbital contributions to the magnetic moment, and μ_{eff} deviates

[a] *Yusuf Hamied Department of Chemistry, University of Cambridge, Cambridge, Lensfield Road, CB2 1EW, Cambridge, UK. E-mail: cpg27@cam.ac.uk*
[b] *The Faraday Institution, Quad One, Harwell Science and Innovation Campus, Didcot OX11 0RA, UK*

† Electronic supplementary information (ESI) available: Methods, Fig. 1 fits, μ_{eff} values, $LiMn_2O_4$ storage, $LiNi_{0.5}Mn_{1.5}O_4$ ICP-OES. See DOI: https://doi.org/10.1039/d2cc06655f

from μ_s when such contributions occur.[28,29] The magnetic moment accounting for orbital contribution is shown in eqn (4), which simplifies to μ_s when $L = 0$ (eqn (3), as $S = n/2$). The μ_{eff} of a sample can also be interpreted *via* comparison to μ_{eff} of known compounds.[29,30]

$$\mu_{S+L} = \sqrt{4S(S+1) + L(L+1)} \quad (4)$$

This work uses ^{1}H BMS shifts of solvent peaks to characterise dissolved transition metals in a typical electrolyte solution, 1 M $LiPF_6$ in 3 : 7 ethylene carbonate : ethyl methyl carbonate (EC : EMC, v/v). Trifluoromethanesulfonimide (TFSI) salts were used to model dissolved Mn^{2+}, Co^{2+}, Ni^{2+}, and Cu^{2+}. NMR spectra of diamagnetic and paramagnetic electrolyte solutions were measured separately (referenced to C_6D_6 capillaries) and the BMS shift was extracted by comparison. Metal dissolution from $LiMn_2O_4$, $LiNiO_2$, and $LiNi_{0.5}Mn_{1.5}O_4$ was characterised by storing cathode powders with electrolyte, after which isolated solutions were analysed with NMR and ICP-OES. Additional experimental details are provided in the ESI,† including a diagram of the NMR tube with solvent capillary (Fig. S1, ESI†).

To evaluate the method's sensitivity, magnetic susceptibility calibration curves were constructed from electrolyte samples containing different concentrations (0.01, 0.05, 0.1, 0.5, 1, 3, and 5 mM) of $Mn(TFSI)_2$ or $Ni(TFSI)_2$ (Fig. 1).

Only the 0.5, 1, 3, and 5 mM measurements are shown in Fig. 1, as the ^{1}H BMS shift upon addition of 0.1 mM of $Mn(TFSI)_2$ or $Ni(TFSI)_2$ is below the limit of detection (LoD) of our experiments; peak shifts at smaller concentrations are negligible. Total magnetic susceptibility χ is presented rather than molar magnetic susceptibility χ_M (*i.e.*, eqn (1) is applied but without dividing by c). Values increase linearly with metal concentration, with good fits from all four peaks (data for fits in (f)–(i) are shown in ESI,† Table S1), indicating that the measurement is reliable for metal concentrations $\geq$0.5 mM.

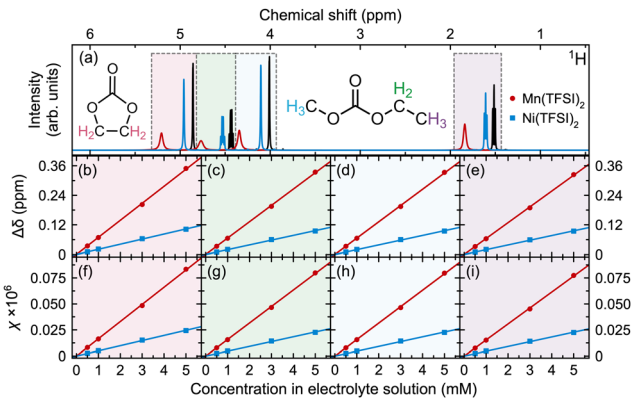

Fig. 1 (a) ^{1}H NMR spectra, (b)–(e) peak shifts, and (f)–(i) magnetic susceptibilities (χ, calculated as in eqn (1) but without dividing by concentration, c), for electrolyte solutions containing $Mn(TFSI)_2$ or $Ni(TFSI)_2$. Spectra are shown for the electrolyte without (black) and with 5 mM Mn^{2+} (red) or Ni^{2+} (blue). Panels correspond to (b) and (f) EC CH_2, (c) and (g) EMC ethyl CH_2, (d) and (h) EMC methyl, and (e) and (i) EMC ethyl CH_3 resonances, shaded with the same colours as used for the protons in the EC and EMC molecules shown in (a).

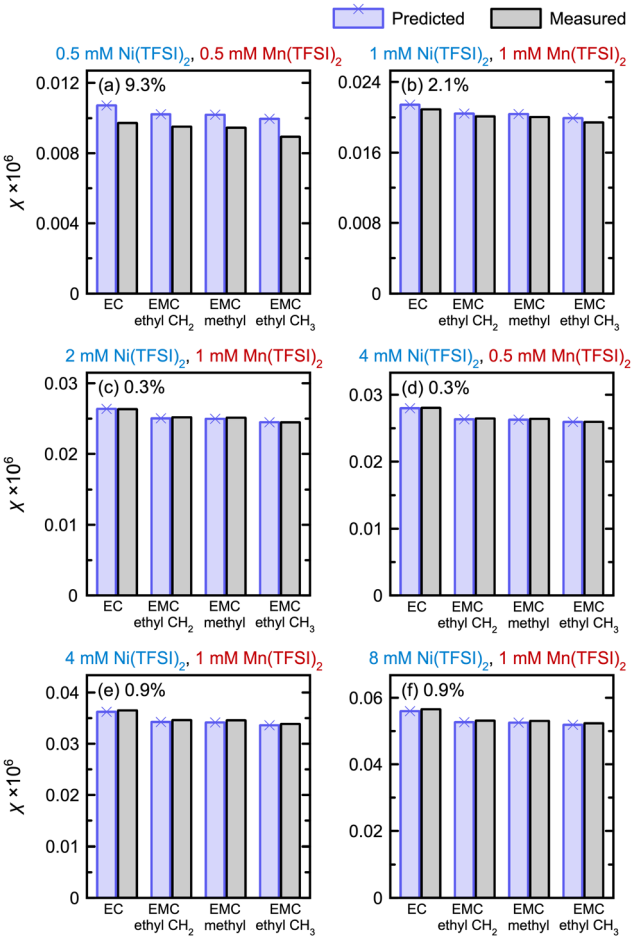

Fig. 2 (a)–(f) Magnetic susceptibilities of solutions containing different amounts of $Mn(TFSI)_2$ and $Ni(TFSI)_2$ added to electrolyte solutions. Percentages give the average error of the four predicted values from the four ^{1}H resonances, as compared to the four measured values for each sample.

The LoD was estimated by calculating μ_{eff} for each sample. At concentrations $\geq$0.5 mM, μ_{eff} = 3.3–3.4 μ_B for Ni^{2+} and 6.0–6.1 μ_B for Mn^{2+}, but this differed by 14–18% at 0.1 mM (3.8 μ_B for Ni^{2+} and 4.9 μ_B for Mn^{2+}); hence, the LoD is in the 0.1–0.5 mM range. We note that small differences in peak positions may arise from small variations in the magnetic field (*e.g.*, from different shimming or placement of samples in NMR tubes) as the diamagnetic and paramagnetic spectra were measured in separate samples and referenced to each other *via* C_6D_6 capillaries. This variation may be reduced by incorporating the diamagnetic and paramagnetic electrolytes into one sample, by using a reference capillary of deuterated diamagnetic electrolyte, which may increase the sensitivity of the method.

To evaluate the method's ability to measure samples containing more than one dissolved metal, solutions were prepared containing both $Mn(TFSI)_2$ and $Ni(TFSI)_2$. Fig. 2 shows the total predicted and observed magnetic susceptibilities of these samples, where predicted magnetic susceptibilities are calculated using the correlations determined in Fig. 1(f)–(i).

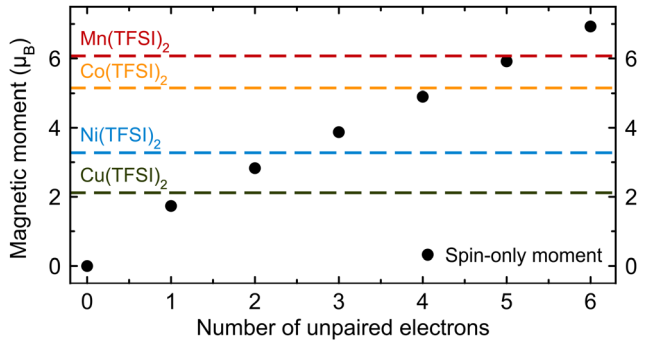

Fig. 3 Effective magnetic moments (dashed lines) for dissolved $Mn(TFSI)_2$, $Co(TFSI)_2$, $Ni(TFSI)_2$, and $Cu(TFSI)_2$, calculated from the BMS shift of the ^1H EMC ethyl CH_3 peak. Black points show the theoretical values of the spin-only magnetic moment for different numbers of unpaired electrons. Electrolyte solutions contained 5 mM $M(TFSI)_2$.

The susceptibilities for samples containing both Ni^{2+} and Mn^{2+} in Fig. 2 are consistent with the calibrations generated from single metals, showing the BMS method is additive. While the error is 9.3% in a solution containing 1 mM paramagnetic ions total, this drops to 2.1% in a solution containing 2 mM paramagnetic ions; all other samples, with 3–9 mM metal ions, have <1% error. Hence, it is important to have a sufficient concentration of metal ions for accurate measurement.

Magnetic susceptibilities were then used to determine magnetic moments (eqn (1) and (2)) for a series of paramagnetic ions often found in battery electrolytes. Fig. 3 shows μ_{eff} for dissolved $Mn(TFSI)_2$, $Ni(TFSI)_2$, $Co(TFSI)_2$, and $Cu(TFSI)_2$ (values listed in ESI,† Table S2), calculated from the EMC ethyl CH_3 shift of 5 mM solutions; μ_s is also shown for comparison.

For d^5 $Mn(TFSI)_2$, μ_{eff} = 6.07 μ_B, which is close to the n = 5 (S = 5/2) value of μ_s, 5.92 μ_B. For $Cu(TFSI)_2$, $Ni(TFSI)_2$, and $Co(TFSI)_2$, $\mu_{eff} > \mu_s$ by 0.38, 0.45, and 1.27 μ_B, respectively. These larger values arise because μ_s does not account for spin–orbit coupling or orbital contributions,[28,29] but for Mn^{2+}, L = 0 and $\mu_{S+L} = \mu_s$ (eqn (3)–(4)). If Co^{2+} (d^7, S = 3/2, L = 3), Ni^{2+} (d^8, S = 1, L = 3), and Cu^{2+} (d^9, S = 1/2, L = 2) were free ions with degenerate d orbitals, all would show orbital contributions to μ_{eff}. If a tetrahedral field splitting occurred, only Ni^{2+} and Cu^{2+} would have an orbital contribution. Instead, the large deviation from μ_s for Co^{2+} only is consistent with an octahedral splitting, where orbital contribution to the magnetic moment is quenched to first order for Ni^{2+} ($t_{2g}^6e_g^2$) and Cu^{2+} ($t_{2g}^6e_g^3$), but not Co^{2+} ($t_{2g}^5e_g^2$).[28] The smaller deviation from μ_s for Ni^{2+} and Cu^{2+} is then due to mixing in of excited states *via* spin–orbit coupling. Although tetrahedral and octahedral splitting are simplifications due to the complex solvation environment, the splitting suggests paramagnetic ions are approximately six-coordinate. The μ_{eff} values in Fig. 3 are also consistent with literature values for these ions.[30] The BMS shift is therefore viable for measuring oxidation states of transition metals in battery electrolyte solutions.

Beyond the BMS shift, additional shifting of select peaks can be induced by coordination to paramagnetic metals *via* the hyperfine shift, which has both contact and pseudocontact (dipolar) components. To compare the reliability of susceptibilities obtained from EC and EMC peak shifts, NEt_4BF_4 was added to the electrolyte solution, since NEt_4^+ is not expected to coordinate to transition metal cations, and χ_M was measured for dissolved $Mn(TFSI)_2$. Table 1 shows magnetic data obtained from comparing diamagnetic and Mn^{2+}-containing electrolyte solutions, both with 0.1 M NEt_4BF_4.

Table 1 ^1H peak shifts and corresponding Mn^{2+} molar magnetic susceptibilities. The peak shift indicates difference between chemical shifts of (i) electrolyte solution + 0.1 M NEt_4BF_4 and (ii) the same solution with 5 mM $Mn(TFSI)_2$ added

	EC	EMC ethyl CH_2	EMC methyl	EMC ethyl CH_3	NEt_4BF_4 CH_2
$\Delta\delta$ (ppm)	0.339	0.326	0.325	0.316	0.315
χ_M (mL mol^{-1})	0.0162	0.0155	0.0155	0.0151	0.0150

Peak shifts in Table 1 follow EC > EMC ethyl CH_2 ~ EMC methyl > EMC ethyl CH_3 ~ NEt_4BF_4 CH_2. The shifts are similar, suggesting all resonances can be used to extract χ_M. However, the EMC ethyl CH_3 resonance shows the smallest $\Delta\delta$ on addition of Mn^{2+} (presumably because it is furthest from the O atoms involved in metal coordination): this shift therefore provides the most accurate χ_M among the solvent peaks. Notably, because the EMC ethyl CH_3 shift is similar to the NEt_4BF_4 CH_2 shift, this shows NEt_4BF_4 addition permits measurement of the BMS shift. The addition of a non-coordinating agent may be beneficial in solutions where solvent peaks are affected by significant hyperfine shifts.

The major contribution to the Mn^{2+} hyperfine shifts likely arises from a contact shift, as high-spin d^5 Mn^{2+} is isotropic[28] so pseudocontact shifts are not possible.[14] This is in contrast to Ni^{2+}, Cu^{2+}, and high-spin Co^{2+}, which may have anisotropic magnetic susceptibilities and may undergo pseudocontact and contact shifts. Peak shifts may also occur due to differences in metal coordination and binding environments within the electrolytes, as observed for Li^+ coordination in carbonate electrolyte solutions, where C and O sites (probed by ^{13}C and ^{17}O NMR) nearer to coordinated Li^+ undergo larger changes in chemical shift on addition of $LiPF_6$.[31,32] Whether arising from a contact or deshielding effect, the larger shift for EC in Table 1 may indicate that Mn^{2+} preferentially coordinates to EC, consistent with previous computational work.[33]

The EMC ethyl CH_3 peak shift was then used to characterise Mn and Ni dissolved from $LiMn_2O_4$, $LiNiO_2$, and $LiNi_{0.5}Mn_{1.5}O_4$ (Fig. 4). Cathode powders were stored with electrolyte and 0.1 vol% water (to generate HF) at 60 °C. (Mn^{2+} dissolution was also observed from $LiMn_2O_4$ stored without added water, ESI,† Fig. S2.) Concentrations from ICP-OES (see below/ESI†) were used to predict the total χ using the calibration in Fig. 1(i).

In all cases, measurements of samples with dissolved Mn and Ni from cathode materials match measurements of samples with dissolved $Mn(TFSI)_2$ and $Ni(TFSI)_2$. The predictions would be inaccurate if the solutions contained dissolved metals with different oxidation states; *e.g.*, Mn^{2+} has μ_s = 5.92 μ_B and $\mu_{eff} \approx$ 5.65–6.10 μ_B;[30] while Mn^{3+} has μ_s = 4.90 μ_B and

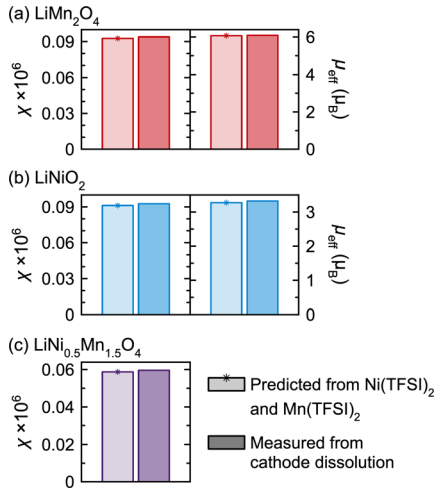

Fig. 4 χ and μ_{eff} for ions dissolved from (a) $LiMn_2O_4$, (b) $LiNiO_2$, and (c) $LiNi_{0.5}Mn_{1.5}O_4$. Predicted arises from $Mn(TFSI)_2$ and $Ni(TFSI)_2$ χ_M values multiplied by ICP-OES concentrations; predicted μ_{eff} values are those reported in Fig. 3 for $Mn(TFSI)_2$ and $Ni(TFSI)_2$.

$\mu_{eff} \approx 4.90–5.00\ \mu_B$.[30] The BMS shift therefore shows that the metals dissolved from $LiMn_2O_4$, $LiNiO_2$, and $LiNi_{0.5}Mn_{1.5}O_4$ are exclusively Mn^{2+} and Ni^{2+}. We note, however, that results may differ depending on the dissolution mechanism (for instance, in a full cell, a high-voltage mechanism may cause dissolution of different species).

If one species is dissolved and χ_M is known, concentration may also be determined (eqn (1)). For $LiMn_2O_4$ and $LiNiO_2$, the peak shift predicts 6.11 mM Mn^{2+} and 20.31 mM Ni^{2+}. ICP-OES of the NMR samples showed 6.03 ± 0.04 mM Mn and 19.98 ± 0.07 mM Ni, respectively. (For $LiNi_{0.5}Mn_{1.5}O_4$ ICP-OES, see ESI†).

In short, we show the oxidation states of dissolved transition metals in battery electrolyte solutions can be determined from simple solution NMR spectra. Even in cases where one metal oxidation state is diamagnetic (*e.g.*, Cu^+, Co^{3+}), the fraction of paramagnetic dissolution can be determined by using the susceptibility of the paramagnetic ion (*e.g.*, Cu^{2+}, Co^{2+}) and solving for its concentration; any remaining metal concentration is then diamagnetic. This accessible method may be applied to any paramagnetic species, making it suitable for lithium-ion and beyond-lithium systems using any liquid electrolyte chemistry. Knowledge of dissolved oxidation states may clarify dissolution mechanisms and dictate strategies adopted to mitigate battery degradation.

This work was funded by the Faraday Institution (grant number FIRG001), the Natural Sciences and Engineering Research Council of Canada, and the Royal Society. JA thanks Evan Zhao for helpful discussions.

Conflicts of interest

There are no conflicts to declare.

References

1 O. C. Harris, S. E. Lee, C. Lees and M. Tang, *J. Phys. Energy*, 2020, **2**(3), 032002.
2 C. Zhan, T. Wu, J. Lu and K. Amine, *Energy Environ. Sci.*, 2018, **11**(2), 243.
3 J. A. Gilbert, I. A. Shkrob and D. P. Abraham, *J. Electrochem. Soc.*, 2017, **164**(2), A389.
4 W. Choi and A. Manthiram, *J. Electrochem. Soc.*, 2006, **153**(9), A1760.
5 Y. Terada, Y. Nishiwaki, I. Nakai and F. Nishikawa, *J. Power Sources*, 2001, **97–98**, 420.
6 R. Sahore, D. C. O'Hanlon, A. Tornheim, C.-W. Lee, J. C. Garcia, H. Iddir, M. Balasubramanian and I. Bloom, *J. Electrochem. Soc.*, 2020, **167**(2), 020513.
7 A. Banerjee, Y. Shilina, B. Ziv, J. M. Ziegelbauer, S. Luski, D. Aurbach and I. C. Halalay, *J. Am. Chem. Soc.*, 2017, **139**(5), 1738.
8 Z. Li, A. D. Pauric, G. R. Goward, T. J. Fuller, J. M. Ziegelbauer, M. P. Balogh and I. C. Halalay, *J. Power Sources*, 2014, **272**, 1134.
9 G. Zhou, X. Sun, Q.-H. Li, X. Wang, J.-N. Zhang, W. Yang, X. Yu, R. Xiao and H. Li, *J. Phys. Chem. Lett.*, 2020, **11**(8), 3051.
10 J. Wandt, A. Freiberg, R. Thomas, Y. Gorlin, A. Siebel, R. Jung, H. A. Gasteiger and M. Tromp, *J. Mater. Chem. A*, 2016, **4**(47), 18300.
11 D. Huang, C. Engtrakul, S. Nanayakkara, D. W. Mulder, S.-D. Han, M. Zhou, H. Luo and R. C. Tenent, *ACS Appl. Mater. Interfaces*, 2021, **13**(10), 11930.
12 Y. Shilina, B. Ziv, A. Meir, A. Banerjee, S. Ruthstein, S. Luski, D. Aurbach and I. C. Halalay, *Anal. Chem.*, 2016, **88**(8), 4440.
13 R. Benedek, *J. Phys. Chem. C*, 2017, **121**(40), 22049.
14 I. Bertini; C. Luchinat; G. Parigi and E. Ravera *NMR of Paramagnetic Molecules: Applications to Metallobiomolecules and Models*, Elsevier, 2016.
15 *EPR Spectroscopy: Fundamentals and Methods*, ed. Goldfarb, D., Stoll, S., John Wiley & Sons, Chichester, UK, 2018.
16 L. Hanf, J. Henschel, M. Diehl, M. Winter and S. Nowak, *Electrophoresis*, 2020, **41**(9), 697–704.
17 L. Hanf, M. Diehl, L.-S. Kemper, M. Winter and S. Nowak, *Electrophoresis*, 2020, **41**(18–19), 1549–1556.
18 L. Hanf, M. Diehl, L.-S. Kemper, M. Winter and S. Nowak, *Electrophoresis*, 2020, **41**(18–19), 1568–1575.
19 D. H. Jang, Y. J. Shin and S. M. Oh, Dissolution of Spinel Oxides and Capacity Losses in 4 V $Li/Li_xMn_2O_4$ Cells, *J. Electrochem. Soc.*, 1996, **143**(7), 2204–2211.
20 L.-F. Wang, C.-C. Ou, K. A. Striebel and J.-S. Chen, *J. Electrochem. Soc.*, 2003, **150**(7), A905–A911.
21 J. Wang, M. M. Islam and S. W. Donne, *Electrochim. Acta*, 2021, **386**, 138366.
22 R. Jung, F. Linsenmann, R. Thomas, J. Wandt, S. Solchenbach, F. Maglia, C. Stinner, M. Tromp and H. A. Gasteiger, *J. Electrochem. Soc.*, 2019, **166**(2), A378–A389.
23 S. Komaba, N. Kumagai and Y. Kataoka, *Electrochim. Acta*, 2002, **47**(8), 1229–1239.
24 T. Joshi, K. Eom, G. Yushin and T. F. Fuller, *J. Electrochem. Soc.*, 2014, **161**(12), A1915–A1921.
25 M. Koltypin, D. Aurbach, L. Nazar and B. Ellis, *Electrochem. Solid-State Lett.*, 2006, **10**(2), A40.
26 D. F. Evans, *J. Chem. Soc.*, 1959, 2003.
27 C. Piguet, *J. Chem. Educ.*, 1997, **74**(7), 815.
28 S. F. A. Kettle, *Coordination Compounds*, Thomas Nelson and Sons, London, 1969.
29 K. Burger, *Coordination Chemistry: Experimental Methods*, The Butterworth Group, London, 1973.
30 B. N. Figgis and J. Lewis. The Magnetochemistry of Complex Compounds, *In Modern Coordination Chemistry: Principles and Methods*, Interscience Publishers, New York, 1960.
31 X. Bogle, R. Vazquez, S. Greenbaum, A. W. von Cresce and K. Xu, *J. Phys. Chem. Lett.*, 2013, **4**(10), 1664.
32 L. Yang, A. Xiao and B. L. Lucht, *J. Mol. Liq.*, 2010, **154**(2), 131.
33 C. Wang, L. Xing, J. Vatamanu, Z. Chen, G. Lan, W. Li and K. Xu, *Nat. Commun.*, 2019, **10**(1), 1.

